Solid State Ionics 190 (2011) 46–52

Contents lists available at ScienceDirect

Solid State Ionics

journal homepage: www.elsevier.com/locate/ssi

Effect of microstructure and catalyst coating on the oxygen permeability of a novel CO_2-resistant composite membrane

Shumin Fang [a], Chusheng Chen [b], Louis Winnubst [a,*]

[a] Inorganic Membranes, IMPACT Institute for Energy and Resources, University of Twente, P.O. Box 217, 7500 AE Enschede, The Netherlands
[b] Laboratory of Materials for Energy Conversion, Department of Materials Science and Engineering, University of Science and Technology of China, Hefei, Anhui 230026, PR China

ARTICLE INFO

Article history:
Received 23 November 2010
Received in revised form 2 February 2011
Accepted 16 March 2011
Available online 19 April 2011

Keywords:
Oxygen permeation
Composite membrane
CO_2-resistant
Doped ceria
Surface-coating

ABSTRACT

Dual-phase membranes based on oxygen-ion-conducting doped ceria and electron-conducting lanthanum chromite show appreciable oxygen flux and good chemical compatibility between the two phases. In this work, $Sm_{0.2}Ce_{0.8}O_{2-\delta}$–$La_{0.7}Ca_{0.3}CrO_{3-\delta}$ (volume ratio 60:40) composite membranes with different grain sizes are prepared. Membranes with large grains (1–5 μm) show much higher permeability than those with small grains (~300 nm). Applying a surface coating of a $Sm_{0.2}Ce_{0.8}O_{2-\delta}$–$Sm_{0.5}Sr_{0.5}CoO_{3-\delta}$ catalyst reduces the running-in time from 220 to several hours and improves the steady-state permeability. The performance of the composite membrane is maintained when applying pure CO_2 as sweep gas, showing promising potential in the application of these membranes in oxyfuel processes using CO_2-diluted oxygen.

1. Introduction

CO_2 capture and sequestration (CCS) in the combustion process of fossil fuels can decrease its contribution to global warming. An efficient method for CCS is the combustion of fossil fuels in CO_2-diluted O_2 generating concentrated CO_2 in the flue stream [1,2]. The CO_2/O_2 mixture can be produced by sweeping CO_2 (recycled from the flue gas) along an oxygen selective membrane which separates oxygen from air. The most important challenges in the development of a membrane for this application are the oxygen permeation performance as well as the mechanical and chemical stability of the membranes under these reactive conditions.

Most research on oxygen selective membranes is focused on perovskite mixed ionic–electronic oxides containing high content of alkaline earth metals, which can easily react with CO_2 [3–5]. Although the stability can be improved by doping with high-valence cations (e.g., Zr and Ti), this strategy also causes loss in permeability [1]. Another type of mixed conductor is a dual-phase composite, which allows oxygen ions and electrons to transport through different phases. Attempts have been made to use electron conducting oxides such as $La_{0.7}Sr_{0.3}MnO_{3-\delta}$, $La_{0.8}Sr_{0.2}CrO_{3-\delta}$, and $Sm_{0.6}Sr_{0.4}Fe_{0.7}Al_{0.3}O_{3-\delta}$ to form composites in combination with the oxygen ion conducting oxides like $Ce_{0.8}RE_{0.2}O_{2-\delta}$ (RE = Gd or Sm) or yttria stabilized zirconia (YSZ) [6–12]. However, during long-term experiments, most of these membranes suffer from loss in flux caused by interdiffusion of cations between the two phases [13]. It is remarkable that $Ce_{0.8}Sm_{0.2}O_{2-\delta}$–$La_{0.8}Sr_{0.2}CrO_{3-\delta}$ (SDC–LSC) shows good compatibility, considerable permeation flux and chemical stability in reducing atmosphere [12,14]. As both Sm-doped ceria and lanthanum chromite have good chemical stability in H_2O and CO_2 [15,16], this composite should also possess high stability in CO_2. Unfortunately, these materials show a long "running-in" time (~200 h) before the permeation flux is stable. In order to shorten the long running-in time, two strategies are tested in this work. Firstly, surface oxygen exchange can be accelerated by decreasing the grain size to sub-micrometer level and thus increasing the length of three phase boundaries (TPBs) among the two solid phases and the gas phase. The surface oxygen exchange process involves both oxygen ionic and electronic charge carriers. As SDC and LSC can be regarded as pure oxygen ionic and electronic conductors, respectively, the reaction only occurs at the TPBs of these composites. Thus it is interesting to compare oxygen permeability of membranes with large and small grains. As the sintering temperature of SDC–LSC membrane is very high (1550 °C for 10 h), a strong grain growth is observed (2–5 μm) [12]. In this work, we try to prepare dual-phase membranes with smaller grains at relatively low temperatures. The sintering temperature to get a relative density of 96% for single phase $La_{0.7}Sr_{0.3}CrO_{3-\delta}$ and $La_{0.7}Ca_{0.3}CrO_{3-\delta}$ is 1700 and 1400 °C, respectively [17]. In order to decrease the sintering temperature and consequently reduce the ceramic grain size we chose $La_{0.7}Ca_{0.3}CrO_{3-\delta}$ as the electronic conducting phase. Fine-grained ceramic powders are prepared to ensure a low sintering temperature. The second method to improve permeation and to reduce the running-in time is by coating the membrane with a porous catalyst layer with high oxygen exchange ability. The performance of perovskite membranes is effectively improved in this way [18–21]. Coating by a porous

* Corresponding author. Tel.: +31 53 4892994.
E-mail address: a.j.a.winnubst@utwente.nl (L. Winnubst).

0167-2738/$ – see front matter © 2011 Elsevier B.V. All rights reserved.
doi:10.1016/j.ssi.2011.03.009

catalyst layer can be even more important in composite membranes because it extends the surface oxygen exchange area from the TPBs of the membrane to the whole surface of the porous catalyst.

In this study, $Sm_{0.2}Ce_{0.8}O_{2-\delta}$–$La_{0.7}Ca_{0.3}CrO_{3-\delta}$ (SDC–LCC) composite membranes with different grain sizes are prepared. The effects of grain size and coating of a catalyst layer on oxygen flux and running-in time are studied. Finally, oxygen permeation behavior and chemical stability in the presence of pure CO_2 are investigated.

2. Experimental

Two types of SDC–LCC membranes were prepared: one with small grain size (denoted as SDC–LCC-1) and the other with larger grain size (SDC–LCC-2). For the fabrication of an SDC–LCC-1 membrane, the starting SDC and LCC powders were prepared via a co-precipitation method and a glycine–nitrate process (GNP), respectively. In the co-precipitation method [22], $Sm(NO_3)_3{\cdot}6H_2O$ and $Ce(NO_3)_3{\cdot}6H_2O$ (Sigma-Aldrich, 99.9%) corresponding to 0.1 mol SDC were dissolved in 1 L deionized water. The solution was heated under stirring at 60 °C. Ammonium hydrogen carbonate (Sigma-Aldrich, 99%) was dissolved in 1 L deionized water in a 2.5 L cylinder vessel. The solution was mildly stirred with a top-mounted turbine stirrer and heated at 70 °C. Agitation was enhanced by the placement of fins along the inside of the vessel. The metal nitrate solution was added dropwise to the precipitant solution at a rate of about 4 mL/min. After aging at the reaction temperature for 1 h, the resultant suspension was filtered via suction filtration. After repeated washing with deionized water and final rinsing with anhydrous ethanol, the precipitate was dried at room temperature under flowing nitrogen and then lightly pulverized with a mortar and pestle before calcination to yield the oxide powders. Calcination of the precipitate was performed under flowing O_2 gas (50 mL/min) in a tubular furnace, using a heating rate of 5 °C/min and a hold time of 2 h at 700 °C. For the synthesis of LCC by the GNP method [23] $CaCO_3$ (Sigma-Aldrich, 99.9%) was dissolved in diluted nitric acid (~10% by weight). Subsequently, $La(NO_3)_3{\cdot}6H_2O$, $Cr(NO_3)_3{\cdot}9H_2O$ and glycine (Sigma-Aldrich, 99%) with an excess of 20% were added and dissolved under stirring. The resultant solution was heated until ignition in small batches so that 1 g powder could be obtained at one time. After combustion, the resultant powder was calcined at 700 °C for 2 h in air in a muffle furnace.

In order to obtain a SDC–LCC-2 membrane with large grains, SDC and LCC powders were prepared via a citrate–nitrate process (CNP) and solid state reaction method (SSR), respectively. In the first process stoichiometric amounts of $Sm(NO_3)_3{\cdot}6H_2O$ and $Ce(NO_3)_3{\cdot}6H_2O$ were dissolved in deionized water under stirring. Citric acid with a citric acid/metal ratio of 2 was added as chelating agent and fuel. This solution was heated under stirring to evaporate water until it turned into viscous gel. The viscous gel was heated until combustion, resulting in fluffy, light yellow powder. The powder was calcined at 850 °C for 3 h in air in a muffle furnace. For the synthesis of LCC by the solid state reaction (SSR), stoichiometric amounts of $CaCO_3$ (Sigma-Aldrich, >99%), La_2O_3 (Sigma-Aldrich, >99.99%) and Cr_2O_3 (Sigma-Aldrich, >99%) were weighed and ball-milled in ethanol for 24 h. The mixture was calcined at 900, 1100 and 1300 °C for 10 h with intermittent ball-milling.

After the required powders were obtained, SDC and LCC (volume ratio 6:4) powders were mixed by ball-milling in ethanol for 24 h. After drying, all obtained powders were uniaxially pressed at 40 MPa, followed by isostatic pressing at 400 MPa for 3 min. Finally, the pellets were sintered at 1200 °C for 1 h and 1500 °C for 20 h for SDC–LCC-1, and SDC–LCC-2 membranes, respectively. The densities of the sintered pellets were measured by Archimedes method in mercury. Detailed sintering studies on cylindrical pellets were performed using a dilatometer (Netzsch Dil-402 C) in air at room temperature to 1500 °C with a heating rate of 2 K/min and a dwell time of 5 h.

The phase composition of the calcined powders and the ceramic microstructure were characterized by powder X-ray diffraction (XRD, Philips X'pert PW1830) and scanning electron microscopy (SEM, JSM-5600LV), respectively.

The oxygen permeation experiments between 850 and 950 °C were performed in a vertical quartz gas permeation system. A disc-shaped sample was sealed into a quartz tube by a glass ring at 1000 °C for 30 min. The effective inner surface area of all membranes was around 0.8 cm^2. After sealing, synthetic air and high purity He were applied to the feed and sweep side of the membrane at a flow rate of 100 and 10 ml/min, respectively. In order to investigate the permeation behavior in CO_2, the sweep gas was switched from He to CO_2 or a mixture of He and CO_2 (volume ratio 1:1) after the flux was stable in air/He gradient. All gas flow rates were controlled by mass flow controllers (Brooks instrument). The effluent gas was analyzed by a gas chromatograph (GC, Varian CP 4900 equipped with 5 Å molecular sieve column using He as carrier gas). The GC was calibrated by standard gas mixtures (O_2 and N_2 in He). The time interval for analysis was normally set at 0.5 h through an auto-injector. The maximum oxygen partial pressure on the sweep side was ~1%, suggesting that the oxygen partial pressure gradient was sufficient. Oxygen leakage, due to imperfect sealing, was evaluated by measuring the nitrogen concentration in the effluent gas. Nitrogen leakage was almost constant in the entire temperature range studied. The leaked oxygen concentration was usually less than 1% of the total oxygen and was subtracted in the calculation of the oxygen permeation fluxes.

A catalyst layer was coated on the feed or sweep side of the membranes in order to accelerate the oxygen exchange process at the surface. For that reason a composite powder of $Sm_{0.2}Ce_{0.8}O_{2-\delta}$ and $Sm_{0.5}Sr_{0.5}Co_{3-\delta}$ (SDC–SSCo, weight ratio 1:1) was synthesized through a combined EDTA–citrate method [24]. After calcination at 1000 °C for 3 h, the powder is mixed with terpineol saturated with methyl cellulose in a weight ratio 2:3. The mixture was milled in agate mortar for 5 h to get a stable slurry. The slurry was dripped or painted on the membrane with a brush to get a loose or relatively dense coating layer. After drying, the membranes were fired at 1000 °C for 3 h.

3. Results and discussion

The sintering behavior of SDC–LCC composites prepared by the two methods is shown in Fig. 1. The influence of the calcination temperature of the LCC powders on sintering behavior of the SDC–LCC-1 green bodies is clearly visible. The composite with LCC calcined

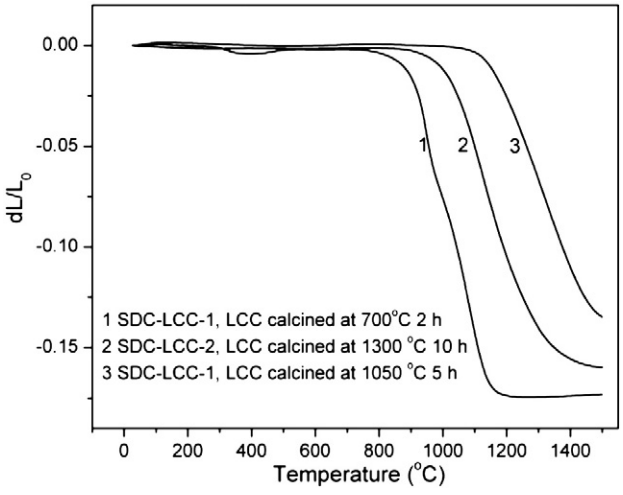

Fig. 1. Sintering behavior of SDC–LCC-1 and SDC–LCC-2 composites from room temperature to 1500 °C at a heating rate of 2 °C/min in air.

at 700 °C shows two shrinkage events which start at 850 °C and 1020 °C, respectively, while a dense ceramic is obtained after heating up to at 1200 °C. However, using the same starting powders but LCC calcined at 1050 °C there is only a shrinkage event which starts at ~1100 °C and is not finished even at 1500 °C. Densification of SDC–LCC-2 (LCC calcined at 1300 °C) starts at ~950 °C and finishes at 1500 °C. To obtain dense membranes with small or large grains, the sintering conditions of SDC–LCC-1 (LCC calcined at 700 °C) and SDC–LCC-2 composites are chosen at 1200 °C for 1 h and 1500 °C for 20 h, respectively.

The XRD patterns of sintered SDC–LCC-1 and 2 membranes are shown in Fig. 2. The main peaks correspond to SDC or LCC in both cases. However, for the SDC–LCC-1 membrane (LCC calcined at 700 °C), peaks corresponding to $CaCrO_4$ (JCPDS no. 08-0458) are also observed. The formation of $CaCrO_4$ is due to Ca solubility limitations in lanthanum chromite at intermediate temperatures [25]. Although the LCC powder after combustion is pure perovskite, $CaCrO_4$ is found in the pattern of an LCC powder calcined at 700 °C but disappears after calcination at 1050 °C for 5 h, which agrees well with the results of Nair et al. [25,26]. $CaCrO_4$ has a melting point of 1022 °C and will dissolve into the perovskite phase with increasing temperature [25]. The formation of a liquid ($CaCrO_4$) phase is beneficial for the sintering and substantially determines the sinterability of the composite. This phenomenon explains the difference in sintering behavior between SDC–LCC-1 samples using LCC powders calcined at 700 and 1050 °C. A dense ceramic is obtained after sintering at ~1200 and >1500 °C for SDC–LCC-1 samples using LCC powders with and without $CaCrO_4$, respectively. In the case of SDC–LCC-2 membranes, LCC powder was calcined at 1100 and 1300 °C for 10 h with intermediate milling and the membranes are sintered 1500 °C for 20 h, which was enough for $CaCrO_4$ to re-dissolve during the calcination process.

Fig. 3a and b shows back-scattered SEM images of these sintered composite membranes with a grain size in SDC–LCC-1 and SDC–LCC-2 of ~300 nm and 1–5 μm, respectively. More pores are observed on SDC–LCC-1 membrane than on SDC–LCC-2 membrane, which is consistent with their relative densities (~90% and 95%, respectively). In the back-scattered mode, the light phase is SDC and the grey phase is LCC. The distribution of the two phases is rather homogeneous, which is beneficial for the percolation of both phases. Fig. 3c and d shows the microstructure of tested SDC–LCC-2 membranes coated with a dense and thin (~20 μm) or a porous and thick (~100 μm) SDC–SSCo catalyst layer on the feed side. The effects of these catalysis coating layers on the performance of SDC–LCC-2 are discussed below.

Fig. 4 displays the time dependence of oxygen fluxes of SDC–LCC-1 and SDC–LCC-2 membranes. The initial flux of the SDC–LCC-1 membrane at 875 °C was 3×10^{-9} mol/cm^{2}s and decreased to zero in 30 h while the flux of SDC–LCC-2 membrane was stable at 2.2×10^{-8} mol/cm^{2}s at 875 °C after a running-in period at 950 °C. Clearly the fine-grained SDC–LCC-1 membrane is not applicable for oxygen permeation. The cause to the degradation is investigated through analysis on the phase composition. The XRD pattern of the SDC–LCC-1 membrane after tests in air/He gradient is shown in Fig. 5a. Peaks corresponding to $CaCrO_4$ and $LaCrO_4$ (JCPDS no. 49-1710) can be observed. The content of these secondary phases increased compared with that of a fresh sample (Fig. 2a) indicating LCC calcined at 700 °C is unstable during the test. The exsolution of $CaCrO_4$ may be unfavorable for oxygen permeation. First, the loss of conducting phases and generation of low-conductive phases decreased the ionic or electronic conductivity of the membrane. Secondly, the resultant $CaCrO_4$ can react with doped ceria forming Ce–Sm–Cr–Ca–O, which also decreased the ionic conductivity [27]. In general, the degradation in performance with time rules out the application of SDC–LCC-1 membrane for oxygen permeation.

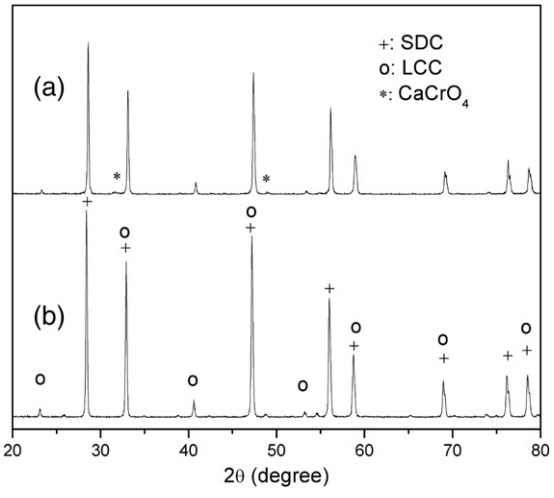

Fig. 2. XRD patterns of SDC–LCC-1 sintered at 1200 °C for 1 h (a) and SDC–LCC-2 sintered at 1500 °C for 20 h (b).

The fluxes of the SDC–LCC-2 membrane without catalyst layer at 950 °C gradually increased from ~3×10^{-9} to 8.5×10^{-8} mol/cm^{2}s in 220 h, which is similar to that observed in SDC—LSC by Yi et al. [12]. It should be mentioned that the membranes didn't break after cooling down from high temperature, suggesting their good mechanical integrity. In the XRD patterns (Fig. 5b and c), the main phases are preserved, while only some minor impurity phases (e.g. $CaCr_2O_4$ and Cr_2O_5) are found probably due to volatilization of Cr. Neither $CaCrO_4$ nor $LaCrO_4$ are found, suggesting that no exsolution of $CaCrO_4$ occurs during the test. SEM images of SDC—LCC-2 membranes tested under air/He gradient are shown in Fig. 6a–d. On the feed side (Fig. 6a), the LCC grains are retained while the large SDC grains turn into small particles (~300 nm). The surface also shows pores (1–2 μm). The increased porosity is beneficial for the length extension of TPBs, and thus the speed of surface reaction might be increased. From the fractured surface close to the feed side (Fig. 6c), it can be seen that the SDC grains on the surface of the feed side are still dense suggesting a very thin porous layer is formed on the feed side. On the surface of permeate side (Fig. 6b), the amount ratio of SDC and LCC is much lower than that of fresh sample. As the residual SDC particles on the sweep side surface is very small, it is reasonable to assume that SDC particles on the surface break into small particles which are blown away by the He flow. It is also noticed that some new phases (not pores, as confirmed on non-shown SEI image) are found. Their size is obviously larger than that of both SDC and LCC grains. Yi et al. also found such new phases and attributed this to the volatilization of Cr [12]. The comparative darkness of the new phases in the back-scattered image indicates that these are probably chromium oxide (Cr_2O_5) or calcium chromite ($CaCr_2O_4$), as indicated by XRD. On the fractured surface close to permeate side (Fig. 6d), the new phases, as observed on the surface, could not be found probably due to their small amount. However, pinholes can be found close to surface in the SDC phase which is light in the backscattered image. These pinholes should be related to the reduction of Ce^{4+} to Ce^{3+} at low oxygen partial pressure and subsequent oxygen release from the lattice. In general, the surface area on both feed and sweep side surfaces increases after a long running-in process, which helps to increase the length of TPBs for surface oxygen exchange reaction.

The “running-in time” significantly decreases by applying a SDC–SSCo catalyst coating. It takes about 1 h and 40 h to obtain a stable oxygen flux when the membrane is coated on sweep and feed side, respectively. In the work of Yi et al., it is shown that a Pt coating on both surfaces of feed and sweep sides also reduces the running-in time to a few hours, but a loss of flux is observed [12]. These results suggest the activation process is surface-controlled because surface coating is very effective in decreasing the running-in time. The fact that coating on the sweep side is more effective indicates that the surface exchange process is predominantly determined by reactions

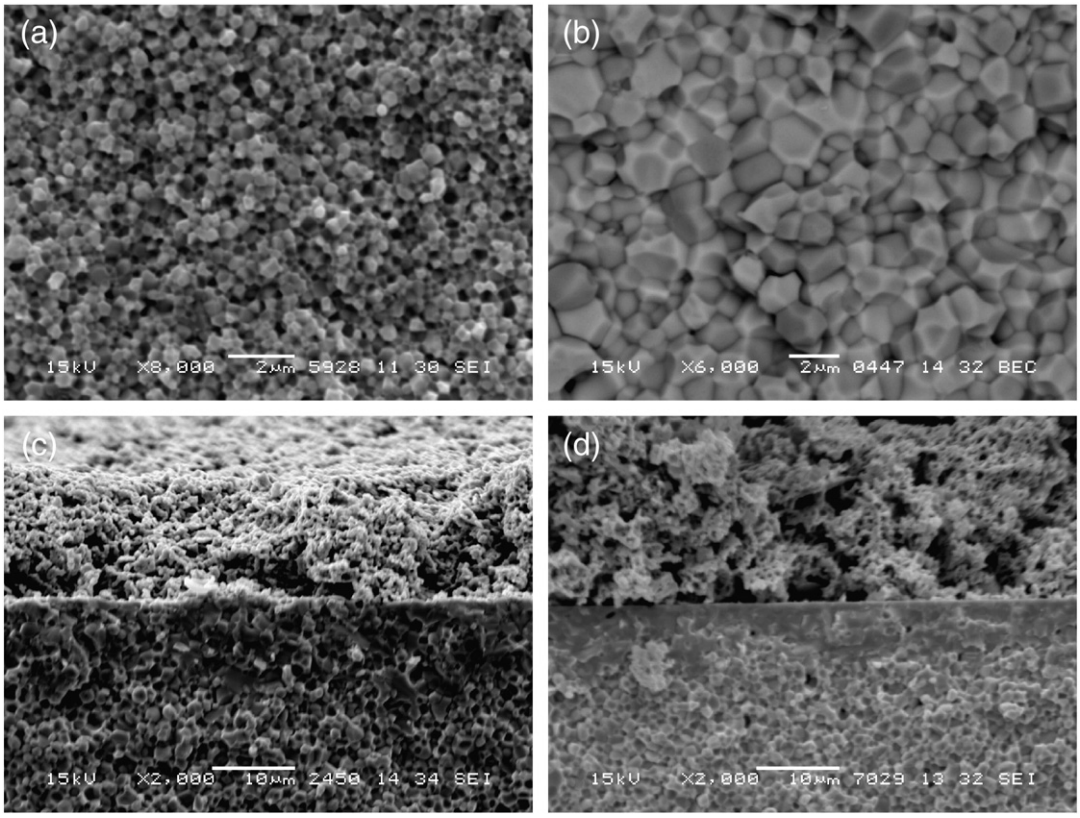

Fig. 3. SEM pictures of several fractured cross sections. (a) SDC–LCC-1 membrane sintered at 1200 °C for 1 h; (b) SDC–LCC-2 membrane sintered at 1500 °C for 20 h without coating layer; (c) tested SDC–LCC-2 with a dense, thin coating layer on the feed side; and (d), tested SDC–LCC-2 with a porous and thick coating layer on the feed side.

at the sweep side surface where oxygen ions are released from lattice forming oxygen molecules.

In order to find whether the running-in process was due to the changes in microstructure during the test, in one experiment the air/He gradient was removed by replacing He with air for 90 h and then switched back to air/He gradient. It can be seen in Fig. 4 that there is still a running-in phenomenon, but the initial oxygen flux is much higher ($\sim 5\times10^{-8}$ compared with 3×10^{-9} mol/cm^{2}s). The difference suggests that microstructural changes of the membrane material during the first running-in period affect the permeation performance.

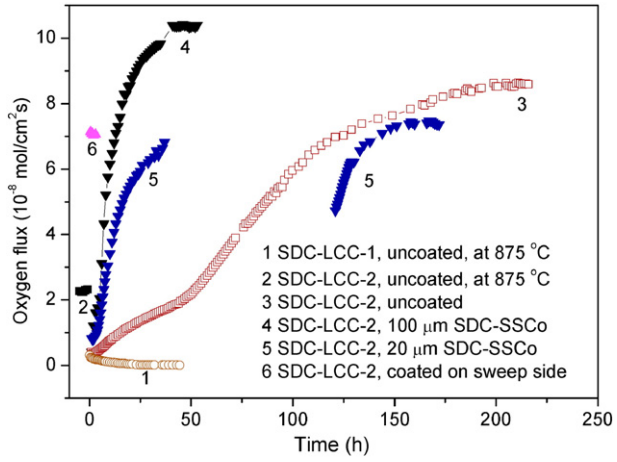

Fig. 4. Time dependence of oxygen flux of SDC–LCC-1 and SDC–LCC-2 membranes with different catalyst layer under air/He gradient. The temperature is 950 °C unless otherwise noted. All membranes are 1 mm thick. All surface catalysts are coated on feed side surface unless otherwise noted. During the measurement of SDC–LCC-2 membrane with 20 μm SDC–SSCo coating layer, He was switched into air at 37 h and switched back at 121 h.

It is noticeable that no running-in process is found for SDC–LSC membrane without coating under air/CO gradient [14], which is similar to the SDC–LCC-2 membrane coated on the sweep side in our study. In [14] it was also shown that exposure to highly reducing CO causes the breakdown of SDC grains, which is also observed when the SDC–LCC-2 membrane reaches equilibrium in our work. The exposure to CO, coating with catalysis layer, or the long-term test all lead to a substantial increase in the area for surface oxygen exchange on the sweep side. These facts indicate that the breakdown of SDC grains and increase in the length of TPBs on the sweep side is responsible for the increase of oxygen permeation flux with time. It can be concluded that the microstructure change determines the running-in time, as it takes

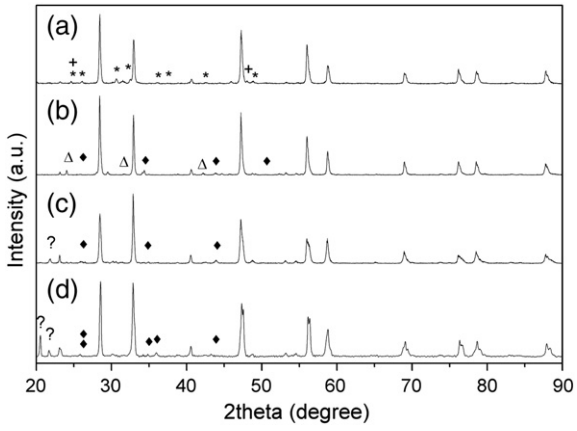

Fig. 5. XRD patterns of composite membranes after tests. (a) sweep side of SDC–LCC-1 membrane, (b) feed side of SDC–LCC-2 membrane, (c) sweep side of SDC–LCC-2 membrane, and (d) sweep side of SDC–LCC-2 membrane tested in CO_2. *: $LaCrO_4$; +: $CaCrO_4$; Δ: Cr_2O_5; ♦: $CaCr_2O_4$; ?: unknown phase.

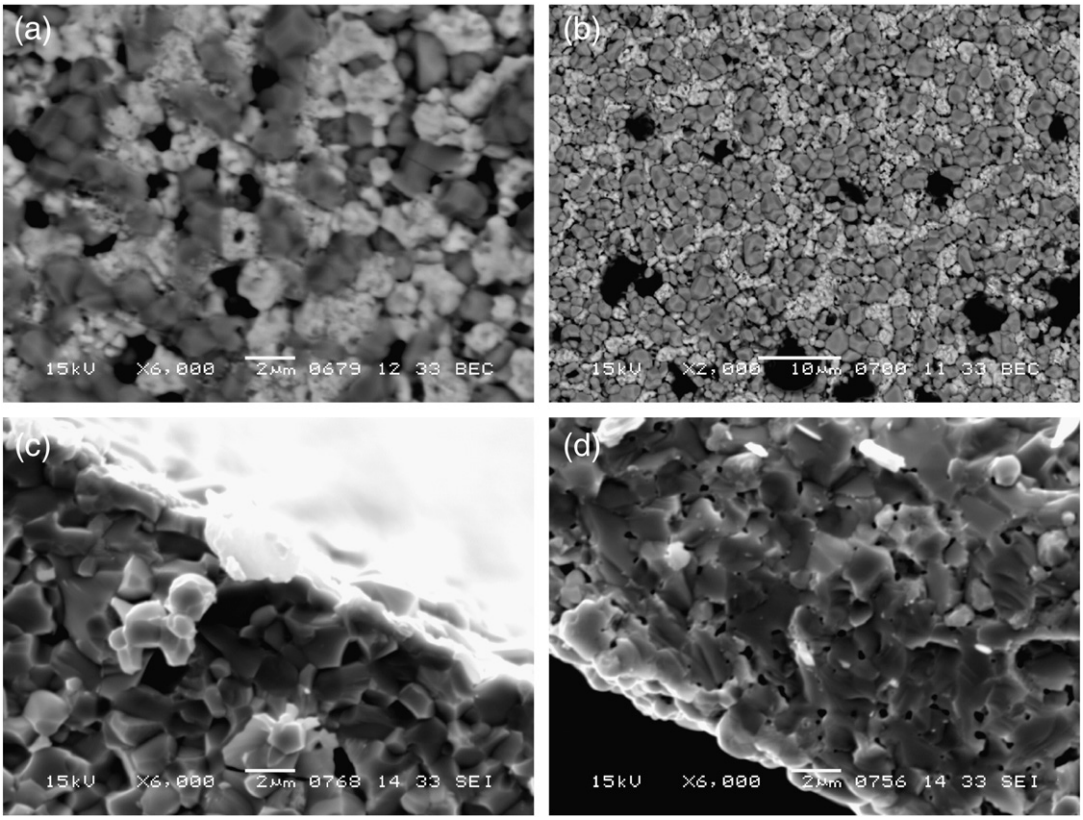

Fig. 6. SEM Micrographs of uncoated SDC–LCC-2 membrane tested under air/He gradient. (a) surface of feed side, (b) surface of permeate side, (c) fractured surface close to feed side, and (d) fractured surface close to permeate side.

0 and 220 h for the equilibrium under CO and He atmosphere, respectively.

The steady-state performance of the membranes is related to the application position and the microstructure of the catalysis layer. When the membrane is coated on the sweep or feed side by a relatively dense and thin catalysis layer (~20 μm, Fig. 3c), the oxygen flux is only 7.1×10^{-8} mol/cm^{2}s, which is ~20% lower than that of uncoated membrane. The application of a thick (~100 μm) and porous SDC–SSCo catalyst on the feed side surface (Fig. 3d) gives the best performance (1.1×10^{-7} mol/cm^{2}s at 950 °C), which is almost identical to the results of $Ce_{0.8}Sm_{0.2}O_{2-\delta}$—$La_{0.8}Sr_{0.2}CrO_{3-\delta}$ as given by Yi et al. [12]. A porous and thick catalyst layer shows higher performance probably due to more channels for gas diffusion and more area for surface reactions. Similar results are observed by Lee et al. when applying porous or dense $La_{0.6}Sr_{0.4}CoO_{3-\delta}$ coating layer on single-phase perovskite $La_{0.7}Sr_{0.3}Ga_{0.6}Fe_{0.4}O_{3-\delta}$ [28,29]. A comparison on the oxygen fluxes of several composite membranes is given in Table 1. Most of these composites show lower oxygen permeation if compared with the SDC–LCC system, studied in this work. Only the performance of GDC–GSF membranes is better.

Table 1
Comparison on the oxygen fluxes at 950 °C of various composite membranes.

Composite composition	Flux (ml min^{-1} cm^{-2})
$Zr_{0.8}Y_{0.2}O_{1.9}+La_{0.8}Sr_{0.2}CrO_{3-\delta}$	0.012 (1.23 mm) [10]
$Zr_{0.84}Y_{0.16}O_{1.92}+La_{0.8}Sr_{0.2}MnO_{3-\delta}$	0.036 (1.18 mm) [30]
$Ce_{0.8}Sm_{0.2}O_{2-\delta}+La_{0.7}Sr_{0.3}CrO_{3-\delta}$ (coated)	0.14 [this study]
$Ce_{0.8}Sm_{0.2}O_{2-\delta}+La_{0.8}Sr_{0.2}CrO_{3-\delta}$	0.13 [12]
$Ce_{0.8}Gd_{0.2}O_{2-\delta}+La_{0.8}Sr_{0.2}MnO_{3-\delta}$	0.038 [31]
$Ce_{0.8}Gd_{0.2}O_{2-\delta}+La_{0.8}Sr_{0.2}Fe_{0.8}Co_{0.2}O_{3-\delta}$	0.085 [32]
$Ce_{0.8}Gd_{0.2}O_{2-\delta}+Gd_{0.7}Ca_{0.3}CoO_{3-\delta}$	0.08 (1.5 mm) [33]
$Ce_{0.8}Gd_{0.2}O_{2-\delta}+Gd_{0.2}Sr_{0.8}FeO_{3-\delta}$ (GDC–GSF)	0.46 [34]

Fig. 7 shows the temperature dependence of steady-state oxygen flux of SDC–LCC-2 membranes without or with a 100-μm-thick catalysis layer after the initial running-in process discussed in Fig. 4 (curve 3 and 4, respectively). The steady-state performance is enhanced by 20–140% between 850 and 950 °C by the catalysis coating. The apparent activation energies for oxygen permeation are 211.0 ± 7.4 and 121.4 ± 2.6 kJ/mol for uncoated and coated membranes, respectively. Similar decrease in activation energy is observed when $La_{0.6}Sr_{0.4}CoO_{3-\delta}$ is

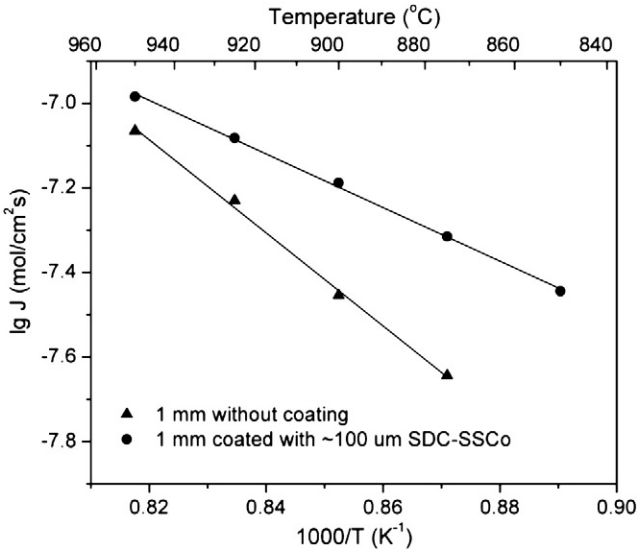

Fig. 7. Temperature dependence of oxygen flux under air/He gradient through 1-mm-thick SDC–LCC-2 membranes with a 100-μm-thick SDC–SSCo catalyst layer or without catalyst layer.

coated on the surface of a $La_{0.7}Sr_{0.3}Ga_{0.6}Fe_{0.4}O_{3-\delta}$ membrane [29]. The enhancement in oxygen permeability based on surface modification is more obvious with decreasing temperature, suggesting the contribution of surface exchange process in the oxygen permeation process is higher at lower temperatures.

Although the membrane coated on the sweep side shows the shortest running-in time, unfortunately, the oxygen flux at 950 °C decreases from 7.1 to 5.3×10^{-8} mol/cm^{2}s in 24 h when the sweep gas is switched to CO_2 (data not shown). The degradation is probably due to the reaction between SSCo phase and CO_2. Partial SSCo is transformed to $SrCO_3$ and Co_3O_4 when it is treated in 25% CO_2 for 50 h at 600 °C [35]. The degradation behavior suggests the SDC–SSCo coating layer cannot be used in the presence of pure CO_2. However, it can be used on the feed side without CO_2. Fig. 8 shows the time dependence of oxygen permeation flux of membrane with SDC–SSCo catalysis layer on the feed side using 50% CO_2/He or 100% CO_2 as sweep gas. After the initial running-in process in an air/He gradient at 950 °C, helium was switched to CO_2 or a mixture of CO_2 and He (volume ratio 1:1) at 900 or 950 °C. First the fluxes increased slightly and then stabilized at the same level of that under air/He gradient. The stable performance in CO_2 suggests that the membrane has a high stability in CO_2. In literature it is reported that $La_{0.85}Ce_{0.1}Ga_{0.3}Fe_{0.65}Al_{0.05}O_{3-\delta}$ was a stable membrane material in a CO_2 environment [36]. However, the permeation fluxes of a 1-mm-thick membrane under air/He and air/He + 20% CO_2 at 950 °C are 1.95 and 1.23×10^{-7} mol/cm^{2}s, respectively, indicating in this case a loss in performance of 30% in the presence of only 20% CO_2 [36]. Although the SDC–LCC composite membrane shows lower permeation fluxes than perovskite membrane, it shows much higher stability in CO_2. Moreover, the performance can be enhanced through the use of higher surface volume ratio of a membrane module, which can be achieved by using a hollow fiber configuration [30].

The XRD pattern of the sweep side surface after a test in CO_2 is shown in Fig. 5d. The main phases are preserved, while some minor secondary phases (e.g. $CaCr_2O_4$, Cr_2O_5) are found. This pattern is similar to that tested under air/He gradient (Fig. 5c). Fig. 9a and b shows the surface and fracture images of CO_2 side, respectively. The surface becomes porous, which is similar to that tested under air/He gradient (Fig. 6b), indicating the exposure to CO_2 does not cause substantial changes in microstructure. The fracture surface image close to the CO_2 side shows a corroded layer with a thickness between 0 and 20 μm. However, this does not lead to the degradation in oxygen permeation flux.

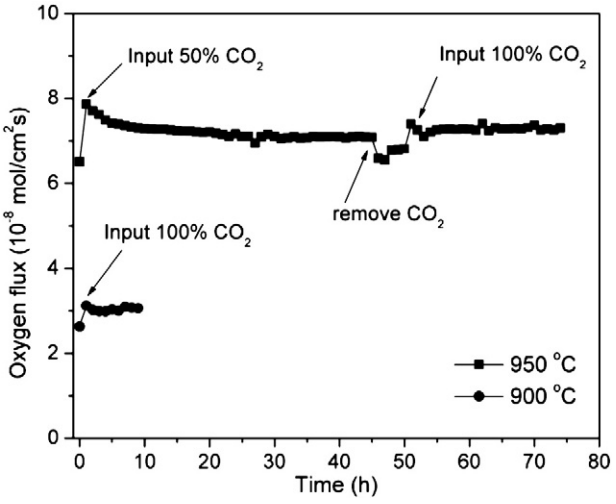

Fig. 8. Time dependence of oxygen fluxes of SDC–LCC-2 membrane in the presence of CO_2 at 950 and 900 °C. Membrane thickness: 1 mm. Coated with 20 μm SDC–SSCo catalyst.

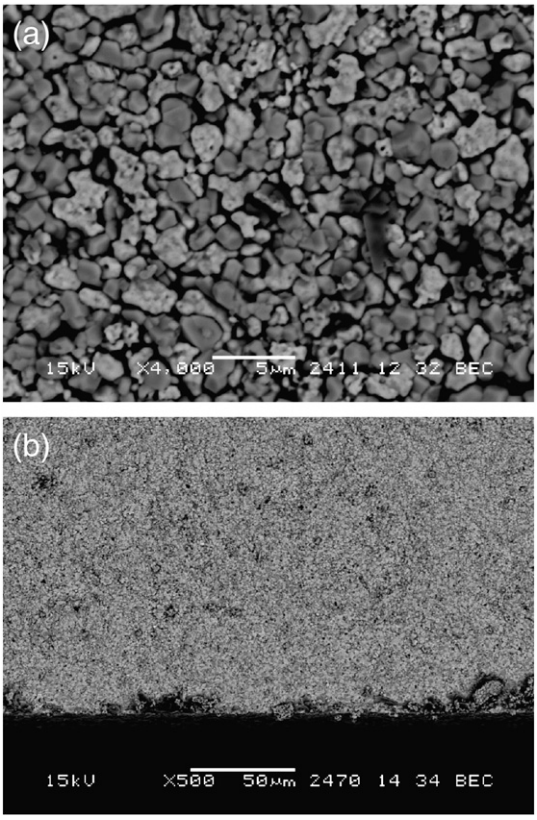

Fig. 9. SEM images of SDC–LCC-2 membrane after test with CO_2 in sweep gas. (a) permeate side surface, and (b) fracture surface image close to the permeate side.

4. Conclusions

The performance of SDC–LCC membranes with small grains decreased with time due to the exsolution of $CaCrO_4$, while the flux of membrane with big grains increased with time due to change on surface microstructure improving surface oxygen exchange. The coating of a porous and thick $Sm_{0.2}Ce_{0.8}O_{2-\delta}$–$Sm_{0.5}Sr_{0.5}Co_{3-\delta}$ catalyst layer on the feed side of membrane can greatly reduce the running-in time, and improve the performance significantly, especially at lower temperatures. The coating of catalyst on the sweep side can eliminate the running-in phenomenon. The membrane showed stable performance in pure CO_2 at 900 and 950 °C, suggesting it as a promising material in the application of CO_2 capture.

Acknowledgements

The authors thank S. Stadman and H.J.G. Klooster for their assistance in the experimental work.

References

[1] Q. Zeng, Y.B. Zuo, C.G. Fan, C.S. Chen, J. Membr. Sci. 335 (2009) 140.
[2] J. Davison, Energy 32 (2007) 1163.
[3] J.X. Yi, S.J. Feng, Y.B. Zuo, W. Liu, C.S. Chen, Chem. Mater. 17 (2005) 5856.
[4] M. Arnold, H.H. Wang, A. Feldhoff, J. Membr. Sci. 293 (2007) 44.
[5] A.Y. Yan, L. Bin, Y.L. Dong, Z.J. Tian, D.Z. Wang, M.J. Cheng, Appl. Catal. B 80 (2008) 24.
[6] V.V. Kharton, A.V. Kovalevsky, A.P. Viskup, A.L. Shaula, F.M. Figueiredo, E.N. Naumovich, F.M.B. Marques, Solid State Ionics 160 (2003) 247.
[7] H. Takamura, K. Okumura, Y. Koshino, A. Kamegawa, M. Okada, J. Electroceram. 13 (2004) 613.
[8] Y. Ji, J.A. Kilner, M.F. Carolan, Solid State Ionics 176 (2005) 937.
[9] A.L. Shaula, V.V. Kharton, F.M.B. Marques, A.V. Kovalevsky, A.P. Viskup, E.N. Naumovich, J. Solid State Electrochem. 10 (2006) 28.
[10] B. Wang, M.C. Zhan, D.C. Zhu, W. Liu, C.S. Chen, J. Solid State Electrochem. 10 (2006) 625.
[11] X.F. Zhu, Q.M. Li, Y. Cong, W.S. Yang, Catal. Commun. 10 (2008) 309.

[12] J.X. Yi, Y.B. Zuo, W. Liu, L. Winnubst, C.S. Chen, J. Membr. Sci. 280 (2006) 849.
[13] V.V. Kharton, F.M.B. Marques, Curr. Opin. Solid State Mater. Sci. 6 (2002) 261.
[14] B. Wang, J.X. Yi, L. Winnubst, C.S. Chen, J. Membr. Sci. 286 (2006) 22.
[15] M. Mogensen, N.M. Sammes, G.A. Tompsett, Solid State Ionics 129 (2000) 63.
[16] J.W. Fergus, Solid State Ionics 171 (2004) 1.
[17] N.M. Sammes, R. Ratnaraj, M.G. Fee, J. Mater. Sci. 29 (1994) 4319.
[18] Y.F. Wang, H.S. Hao, J.F. Jia, D.L. Yang, X. Hu, J. Eur. Ceram. Soc. 28 (2008) 3125.
[19] T.H. Lee, Y.L. Yang, A.J. Jacobson, B. Abeles, S. Milner, Solid State Ionics 100 (1997) 87.
[20] G. Etchegoyen, T. Chartier, P. Del-Gallo, J. Solid State Electrochem. 10 (2006) 597.
[21] W.K. Hong, G.M. Choi, J. Membr. Sci. 346 (2010) 353.
[22] J.G. Li, T. Ikegami, T. Mori, T. Wada, Chem. Mater. 13 (2001) 2913.
[23] L.A. Chick, L.R. Pederson, G.D. Maupin, J.L. Bates, L.E. Thomas, G.J. Exarhos, Mater. Lett. 10 (1990) 6.
[24] W. Zhou, Z.P. Shao, W.Q. Jin, J. Alloys Compd. 426 (2006) 368.
[25] L.A. Chick, J. Liu, J.W. Stevenson, T.R. Armstrong, D.E. McCready, G.D. Maupin, G.W. Coffey, C.A. Coyle, J. Am. Ceram. Soc. 80 (1997) 2109.
[26] S.R. Nair, R.D. Purohit, A.K. Tyagi, P.K. Sinha, B.P. Sharma, Mater. Res. Bull. 43 (2008) 1573.
[27] C.E. Hatchwell, N.M. Sammes, G.A. Tompsett, I.W.M. Brown, J. Eur. Ceram. Soc. 19 (1999) 1697.
[28] K.S. Lee, S. Lee, J.W. Kim, S.K. Woo, Desalination. 147 (2002) 439.
[29] S. Lee, K.S. Lee, S.K. Woo, J.W. Kim, T. Ishihara, D.K. Kim, Solid State Ionics 158 (2003) 287.
[30] W. Li, J.-J. Liu, C.-S. Chen, J. Membr. Sci. 340 (2009) 266.
[31] V.V. Kharton, A.V. Kovalevsky, A.P. Viskup, F.M. Figueiredo, A.A. Yaremchenko, E.N. Naumovich, F.M.B. Marques, J. Electrochem. Soc. 147 (2000) 2814.
[32] A.L. Shaula, V.V. Kharton, F.M.B. Marques, A.V. Kovalevsky, A.P. Viskup, E.N. Naumovich, Br. Ceram. Trans. 103 (2004) 211.
[33] U. Nigge, H.D. Wiemhofer, E.W.J. Romer, H.J.M. Bouwmeester, T.R. Schulte, Solid State Ionics 146 (2002) 163.
[34] X.F. Zhu, W.S. Yang, Aiche J. 54 (2008) 665.
[35] H. Zhang, Y. Cong, W. Yang, Chin. J. Catal. 29 (2008) 7.
[36] X.L. Dong, G.R. Zhang, Z.K. Liu, Z.X. Zhong, W.Q. Jin, N.P. Xu, J. Membr. Sci. 340 (2009) 141.